Implementation of *In-Situ* Impedance Techniques on a Full Scale Aero-Engine System

R. J. Gaeta*
Georgia Institute of Technology, Atlanta, Georgia 30332-0844

J. M. Mendoza†
Honeywell Aerospace, Phoenix, Arizona 85034

M. G. Jones‡
NASA Langley Research Center, Hampton, Virginia 23681-2199

Determination of acoustic liner impedance for jet engine applications remains a challenge for the designer. Although suitable models have been developed that take account of source amplitude and the local flow environment experienced by the liner, experimental validation of these models has been difficult. This is primarily due to the inability of researchers to faithfully mimic the environment in jet engine nacelles in the laboratory. An *in-situ* measurement technique, one that can be implemented in an actual engine, is desirable so an accurate impedance can be determined for future modeling and quality control. This paper documents the implementation of such a local acoustic impedance measurement technique that is used under controlled laboratory conditions as well as on full scale turbine engine liner test article. The objective for these series of *in-situ* measurements is to substantiate treatment design, provide understanding of flow effects on installed liner performance, and provide modeling input for fan noise propagation computations. A series of acoustic liner evaluation tests are performed that includes normal incidence tube, grazing incidence tube, and finally testing on a full scale engine on a static test stand. Lab tests were intended to provide insight and guidance for accurately measuring the impedance of the liner housed in the inlet of a Honeywell Tech7000 turbofan. Results have shown that one can acquire very reasonable liner impedance data for a full scale engine under realistic test conditions. Furthermore, higher fidelity results can be obtained by using a three-microphone coherence technique that can enhance signal-to-noise ratio at high engine power settings. This research has also confirmed the limitations of this particular type of *in-situ* measurement. This is most evident in the installation of instrumentation and its effect on what is being measured.

Nomenclature

c	speed of sound
h	honeycomb depth
k	wave number
M_{gr}	Grazing Mach number
P	acoustic pressure
R	acoustic resistance
u	acoustic velocity
X	acoustic reactance
z	specific acoustic impedance
ρ	density

*Senior Research Engineer, Georgia Tech Research Institute; Associate Fellow AIAA.
†Principal Engineer, Associate Fellow AIAA.
‡ Senior Research Scientist; Senior Member AIAA

ω	angular frequency
ϕ	phase difference between face sheet and back wall

I. Introduction

Determination of acoustic liner impedance for jet engine applications remains a challenge for the designer. Although suitable models have been developed that take account of source amplitude and the local flow environment experienced by the liner[1-3], experimental validation of these models has been difficult. This is primarily due to the inability of researchers to faithfully mimic the environment in jet engine nacelles in the laboratory. Thus, methodologies for measuring acoustic liner impedance *in situ* are sought by designers. This is the basis for the work presented in this paper.

A. Objectives of the EVNERT Program

The measured data and corresponding test background information to be provided in the current paper are from the Honeywell-led Engine Validation of Noise and Emission Reduction Technologies (EVNERT) program. The intent of this program is to advance engine noise reduction technologies to a Technology Readiness Level (TRL) of 5 for Phase 1 and to demonstrate/validate inlet and exhaust advanced source diagnostic methods. A Honeywell-led team consisting of NASA, other industry partners, and academia was established for this program. The objective for the present work was to demonstrate the efficacy of making local, *in-situ* impedance measurements on an installed liner. *In-situ* impedance measurements will substantiate treatment design, provide understanding of flow effects on installed liner performance, and provide modeling input for fan noise propagation computations.

Honeywell, NASA Langley, and the Georgia Tech Research Institute (GTRI) have conducted a series of acoustic liner evaluation tests for this study: (1) *in-situ* and two-microphone method tests in a normal incidence impedance tube, (2) *in-situ* and impedance eduction method tests in a grazing flow impedance tube, and (3) *in-situ* testing in a full scale engine nacelle during ground tests. The first of these tests were essentially risk mitigation steps. Lab tests were intended to provide insight and guidance for accurately measuring the impedance of the liner housed in the inlet of a Honeywell Tech7000 turbofan. This engine is shown in **Fig 1** and some engine performance and geometric parameters for this engine are indicated in **Table 1**. The *in-situ* diagnostic technique was implemented with the engine operating on a static test stand.

B. Reliable, Robust, Simple Liner Impedance Determination

The design of acoustic liners for aero-engine applications relies on optimizing specific acoustic impedance for a given fan, turbine, and inlet/nozzle configuration. Once the optimum impedance is determined, the liner is designed and fabricated and the resultant liner impedance is experimentally determined. Impedance determination can be obtained by a variety of methods. A common and simple method uses a normal incidence impedance tube to provide rapid determination of the liner impedance under normal plane wave incidence. Several impedance tube techniques exist, but the accepted method is the so-called Two-Microphone Method (TMM) that is outlined in the ASTM Standard E1090-98[4] and follows the original work of Chung and Blaser[5].

However, the normal incidence impedance tube doesn't account for effects of grazing incidence and grazing flow on the liner impedance. The latter effect is substantial, especially for the resonant class of liners most commonly used on aero-engines. Many studies[6-10] have shown the strong effects of a grazing flow field on the impedance of a resonant liner, specifically in how it affects the liner's optimum impedance for a specific duct. In order to assess the performance under a velocity boundary layer, a liner is typically installed in a flow duct as part of the wall. There are two fundamental ways to experimentally determine liner impedance under grazing flow. One is to establish a controlled environment in a flow duct where fluctuating pressures can be measured and impedance calculated. The other is to make these measurements in the actual installed configuration (*in-situ*), e.g., an aero-engine. The former technique has the distinct advantage of controllability. The experimental methods can be adjusted to the facility particulars such as duct size, liner access, and typically more robust (non-flight worthy) hardware. *The in-situ* technique allows measurements in actual aero-engines, but must maintain more flexibility than required in the former technique. The ideal and desired technique would be one that could be used in the controlled laboratory flow duct environment *and* in an actual engine installation.

C. Dean's *In-Situ* Technique – Critical Experimental Assumptions

Historically, the measurement of liner impedance in grazing flow has utilized a wave guide or impedance tube placed perpendicular to the flow duct/liner installation[6,7,11]. These methods had the advantage of not needing measurements near or in the duct flow field. The big disadvantage is that it is nearly impossible to apply the tube in an actual engine configuration and the methodologies require precise calibration. A big step forward was taken with the publication of Dean's seminal paper[12] where he extended the methods of Phillips[13] and Binek[14] to the measurement of localized, *in-situ*, impedance of resonant liners† (liners consisting of honeycomb cells with perforated face sheets). Using only two microphones placed in strategic places for a single-degree-of-freedom liner, Dean demonstrated a technique that could be used in laboratory flow ducts as a method of determining impedance under a grazing flow environment. It was easy to see how it could be used on an actual engine installation without significant changes. Furthermore, the *in-situ* method lends itself to liner model and design validation as it can be used in zero flow normal incidence impedance tubes, laboratory flow ducts, and actual engine configurations. Several other researchers have used the *in-situ* technique,[15-17] most notably Zandbergen, et al who implemented it on the engine of a Fokker F28 aircraft for flight testing. Finally, the *in-situ* technique applied to an installed engine liner can enable the real-time tracking of impedance, which lends itself to an actively controlled system.

Other techniques have been under development for over 15 years, notably NASA Langley's method of extracting liner impedance from flow duct boundary condition measurements[18]. This has been implemented in laboratory flow ducts but remains under investigation for use with actual engine configurations. A key distinction of the *in-situ* technique relative to other measurement techniques is that it measures the *local* liner impedance. Usually liners are designed to exhibit uniform impedance, but manufacturing abnormalities prevent attaining this uniformity. Moreover, the very nature of bonding a perforated face sheet to honeycomb intrinsically makes the geometry of each honeycomb cell slightly different. Over a large liner area, these local geometry differences average out, but *in-situ* measurements measured at a particular cell produce a local result. **Fig 2** shows the basic assumptions and computational method for the in situ measurement technique as developed by Dean. Inside the cavity, the incident pressure wave represented by:

$$P_{+} = P_o e^{i(\omega t - ky)} \tag{1}$$

And the reflected wave represented by:

$$P_{-} = P_o e^{i(\omega t + ky)} \tag{2}$$

Yields an expression for a standing wave in the cavity:

$$P = 2P_o e^{i\omega t} \cos(ky) \tag{3}$$

With the cavity covered with some thin damping material, the particle velocity normal to the liner can be expressed as:

$$u = -i\frac{2P_o}{\rho c} e^{i\omega t} \sin(ky) \tag{4}$$

Normalized to ρc, the impedance in terms of the acoustic pressure at the liner surface and the back wall is:

$$z = \frac{P_{face-sheet}}{u_{face-sheet}} = -i\frac{P_{face-sheet}}{P_{back-wall}} e^{i\phi} \sin^{-1}(kh) \tag{5}$$

† Point of clarification: The two-microphone in-situ technique popularized by Dean should not be confused with the Two Microphone Method (TMM), which is a cross-correlation technique commonly used for impedance tube results (ASTM E1050). This paper will use the *"in-situ technique"* and *"Dean's method"* interchangeably and use *"TMM"* when referring to the cross-correlation technique.

Where h is the liner depth and ϕ is the phase angle between the face sheet acoustic pressure and the back wall acoustic pressure.

II. Preliminary Normal Impedance Experiments

A. Objectives and Technical Approach

As a way of mitigating risks inherent in the planned full scale engine tests, as series of normal incidence impedance tube tests were performed at GTRI facilities to checkout proposed *in situ* instrumentation and measurement technique. The objective of this testing was two-fold: 1) To compare and checkout the *in situ* methodology relative to the TMM and 2) to determine the effect of instrumentation placement on the measured impedance.

The acoustic liner under consideration is a single degree-of-freedom (SDOF) resonant liner comprised of a honeycomb layer with a face sheet bonded to one side and a rigid aluminum backing on the other side. **Fig 3** shows the general features of this liner as designed by Honeywell.

The face sheet consists of a perforate with a wire mesh screen bonded to one side. **Fig 4** shows this face sheet's geometric details. The perforate was 0.032 inches thick, had holes that were 0.050 inches in diameter on staggered centers. This results in a nominal porosity (open area) of 13%. These holes were discernable from the wire mesh side as well. The nominal honeycomb layer thickness was 0.625 inches.

Preliminary tests were conducted in a normal incidence impedance tube where the TMM technique and the *in situ* technique were employed simultaneously. The face sheet was placed in the impedance tube with the wire mesh side facing the sound source (as would be in the engine installation) with a 0.7 inch air gap behind it. This configuration differed from the actual liner only in the lack of discrete honeycomb cells. Both broadband and single tones were introduced into the tube.

B. Instrumentation

Impedance Tube

The normal incidence impedance tube used is approximately 20 inches long and 1.12 inches in diameter (ID). The diameter of the tube dictates that plane wave data can be acquired up to 6400 Hz. The acoustic source is a JBL[‡] 2446J compression driver. The tube uses two B&K phase-matched ¼-inch microphones in a TMM arrangement to determine impedance of a sample placed at the end of the tube. **Fig 5** shows this impedance tube. Acoustic signals from these microphones are manipulated in a Labview program that uses procedures outlined in ASTM E1050-98[4] to compute the impedance and absorption coefficient.

In Situ Instrumentation

The most crucial aspect to implementing the in situ impedance measurement technique is the installation of the appropriate instrumentation. Delicate, sensitive, and small microphones must be placed in very cramped and harsh environments while producing good signal-to-noise ratios and representative acoustic data. Initially, Kulite XCE-062 microphones were used for the in situ measurements. It was discovered that the wire shielding provided by the manufacturer was inadequate and produced low signal-to-noise ratios, thus compromising the integrity of the data. The Endevco Model 8507C-2 piezoresistive microphone offered much better EMI shielding and was the microphone of choice for this study. These microphones have a nominal maximum outer diameter of 0.090 inches. They have manufacturer-stated range of 100 dB to 181 dB with an operating temperature up to 200 ^{0}F. The frequency range is DC to 15 kHz. In practice, the lower amplitude range has been shown to be close to 85 dB. However, as will be shown, further signal enhancement was needed in the form of filtering. The Endevco microphones were sheathed in a brass tube for ease of installation and to add some ruggedness. The signals from the Endevco microphones are condition with instrumentation amplifiers before being input into a 16 channel Data Physics Abacus signal analyzer.

In Situ Microphone Calibration

[‡] The brand names of instrumentation used in this paper in no way is meant to be an endorsement of that particular brand by NASA, Honeywell, or GTRI. It is provided to aid the reader's understanding of the test approach.

In the application of the *in situ* method, it is crucial that the microphones at the face sheet and the back wall are phase matched. If they are not, a calibration must be performed to correct for any phase mismatch as a function of frequency. The phase characteristics for the Endevco microphones were assessed using the normal incidence impedance tube. By placing the Endevco microphone in the same acoustic pressure field as a standard B&K ¼-inch microphone, the phase relationship amongst Endevco transducers can be discerned. **Fig 6** shows a backing plate that has both a flush-mounted B&K microphone and an Endevco. This set up was used to obtain amplitude and phase characteristics. The B&K microphone was tested with and without its protection grid and no discernable difference in the response was measured, thus the grid was left on for most all of the calibration tests conducted. **Fig 7** shows the results of several Endevco transducer phase calibrations. It is clear that there is excellent phase agreement inherent in these transducers and **Fig 8** shows that the differences are less than +/- 0.5 degrees between those tested. Furthermore, there is less than 1 dB of difference in the amplitude calibration. **Fig 9** shows a typical amplitude calibration response over the applicable frequency range.

D. Normal Impedance Tests

Checkout of the In Situ Methodology

The perforated face sheet was placed at the reference plane of the impedance tube. An air gap of approximately 0.7 inches was set behind the face sheet. Initial tests placed the face sheet Endevco microphone in between perforate holes. A flush mounted Endevco was placed on the hard back wall. **Fig 10** shows how the face sheet is fit into the impedance tube. **Fig 11** shows how the Endevco microphones are installed in the face sheet and the back wall of the air gap to obtain the relevant acoustic data for the *in situ* impedance calculations. These data result from the face sheet microphone being placed in between perforate holes.

The TMM was used simultaneously with the in situ method and was used as a reference to compare the impedance. **Fig 12** shows the measured impedance of the face sheet with air gap using the *in situ* technique for along with the TMM data for comparison. There is very good agreement between the TMM results where the face sheet microphone is between two adjacent holes. As expected, the *in-situ* method measures a higher resistance when the microphone takes the place of one of the holes.

Effect of Microphone Face Sheet Placement

The effect of putting the face sheet microphone in between perforate holes (configuration #1) and within one of the perforate holes (configuration #2) was examined. It is observed that the reactance is not affected appreciably, however there is a noticeable difference in the resistance (see Fig 12). When one of the holes is replaced with a microphone (configuration #2), the resistance is artificially increased as expected. The very tight dimensions between holes, given the size of the microphone, make only these two configurations possible. Because the spacing within an actual honeycomb cell is tight, it was recommended that the face sheet microphone be placed within one of the perforate holes (Configuration #2) when installing the instrumentation on the grazing flow test liner and full scale engine liner. The tolerances of drilling holes in the face sheet were not tight enough to allow the microphone hole from "breaking" into adjacent holes. It would be left for the data to be adjusted for this artificially increased resistance due to a decreased local effective porosity.

III. Grazing Flow Experiments

A series grazing flow experiments were undertaken to mitigate the risks of testing on the full scale Tech7000 engine. It has been established in previous experiments using the Dean method of *in situ* impedance determination that the results are very sensitive to instrumentation performance and installation effects. With this in mind, a representative honeycomb liner was fabricated with the same type of linear face sheet that was used in the preliminary impedance tube experiments. This liner was then placed in NASA's Grazing Flow Impedance Tube (GIT) where it was tested under controlled duct velocity and sound pressure level conditions. Furthermore, testing in the GIT provided an assessment of using a coherence based technique to separate unwanted hydrodynamic noise from the acoustic noise (effectively enhancing the signal-to-noise ratio of the data). Impedance of the sample liner was determined using NASA's eduction technique (see ref.18) while data was simultaneously acquired for in situ calculations for comparison. These experiments shed light on the difficulties that can arise when trying to implement Dean's Method in practical situations.

In addition, a limited number of normal incidence impedance tube tests were performed in NASA's Normal Incidence Tube Facility (NIT). These measurements were done "*in-situ*" that is, the test liner was clamped against

the opening of the impedance tube during measurement. This is a common technique when dealing with honeycomb liners but it does raise some interesting questions about acquiring accurate results. This testing led to similar testing performed at GTRI to shed light on potential inaccuracies using this methodology.

A. Experimental Set up and Data Processing Procedure

NASA's GIT facility

A single-degree-of-freedom liner was fabricated to fit into NASA Langely Research Center's Grazing Incidence Tube. This 20-foot long, 2-inch by 2-inch waveguide measures acoustic liner performance under a controlled grazing flow environment. As shown in the photograph of NASA's GIT (**Fig 13**), air flows from left to right through the test section, in which the upper wall contains the acoustic liner. Heated, pressurized air is supplied at the duct entrance via a plenum chamber, and is combined with a vacuum pump at the duct exit to allow testing in the test section at near-ambient conditions. Four 120-W electromagnetic acoustic drivers mounted upstream of the plenum provide the desired acoustic source. The plenum is designed to allow optimum merging of the acoustic and mean flow fields, such that tests can be conducted at grazing flow Mach numbers up to 0.5 and with single tone SPL's up to at least 140 dB from 500 to 3000 Hz.

Data Acquisition and Processing

GTRI fabricated a special signal conditioning box that powers the Endevco microphones and amplifies their signals. GTRI also provided a portable Data Physics Abacus multi-channel signal analyzer that was used to process signals from the Endevco microphones. Signals from these liner microphones were also input into NASA's data acquisition system where only the time histories were recorded for later processing.

Signal Enhancement: Three-Microphone Methodology

One objective of the GIT tests was to evaluate the 3-Microphone methodology as a way of increasing the signal-to-noise ratio. As applied to the in situ measurements, this method utilizes the two microphones in a particular honeycomb cell with another microphone that is flush mounted to the liner face sheet at another location. In the GIT test configuration, the third face sheet microphone was a microphone flush mounted to the face sheet midway between the LE and TE locations. This method uses coherence functions between the chosen microphones to compute correlated auto-spectra to be used for Dean's in situ impedance method. Details of the signal processing algorithms can be found in reference 19. **Fig 14** shows a notional diagram of how these three microphones might be arranged to achieve signal enhancement.

NASA personnel operated the facility and acquired data from 95 B&K quarter-inch microphones along with pressure and temperature measurements to analytically educe the impedance of the liner. A Cytec switch is combined with multiple high-speed Agilent Technologies E1432 A/D converters to acquire the data. The switch allows data to be acquired with 48 microphones at a time (the reference microphone is sampled twice). A LabView routine is used to control the data acquisition, and to perform spectral analysis to determine the SPL and phase at each microphone location. These results are stored for off-line analysis via finite element methods. For the current study, only the 31 microphones located on the wall opposite of the liner were used to educe the impedance. These data were acquired simultaneously with the *in-situ* measurements, such that the results from the two approaches could be compared directly.

Test Plan

Tests were conducted at three grazing flow Mach numbers (0.0, 0.30, 0.475) with two types of sources (broadband, sinusoidal tones) at three nominal sound pressure levels (broadband, 120 dB, 140 dB). Tones were introduced from 400 Hz to 3000 Hz at 200 Hz intervals..

B. Liner Fabrication

A test liner was fabricated using a wire mesh/perforate face sheet bonded to 3/8-inch honeycomb cell that was provided by Honeywell. The wire mesh was stainless steel and had a nominal resistance of 10 Rayls. It was bonded to a perforate which had a nominal thickness of 0.032 inches, 0.050 inch diameter holes producing a sheet open area of 13.5%. The thickness of the liner was approximately 1.5 inches. This was chosen so the liner resonance frequency would be less than 3000 Hz which is the cut-on frequency of NASA's GIT. A backing plate was fabricated from 1/8" aluminum and bonded to the back of the test honeycomb liner.. **Fig 15** shows the face sheet microphone location relative to the honeycomb cell as seen from the back side of the liner while **Fig 16** shows the

transducer from the grazing flow side. Two locations on the liner were chosen for the *in-situ* calculations. One near the LE of the liner and one near the TE. In addition, a flush face sheet microphone was placed in the center of the liner to act as a correlating signal to separate the flow noise from the *in-situ* measurement. **Fig 17** shows this installation in the GIT.

C. Grazing Incidence Tube Results

Normal Incidence Check-out Tests

Before the liner was shipped to NASA, GTRI performed normal incidence impedance tests (using the TMM to determine impedance). This was for comparisons with NASA data. **Fig 18** shows the liner clamped to the end of GTRI's 1.13" diameter normal incidence impedance tube (NIT). **Fig 19** shows the resulting comparison of impedance as measured with the TMM at GTRI and NASA. Note that while the agreement in reactance is reasonable above the resonance condition, very poor agreement exists at other frequencies. Poor agreement exists with the resistance as well.

These TMM results were interesting enough to force GTRI to build an impedance tube that mimicked the NASA NIT as closely as possibly. A 2"x2" aluminum tube with 0.25" wall thickness was purchased and cut to a length matching the NASA tube. Flush mounted microphones were placed in identical positions as NASA's. GTRI used the same acoustic driver as NASA, however only one was used where NASA uses up to 6 drivers. The liner was clamped to the new GTRI tube much like it was for the smaller tube. **Fig 20** shows the resulting impedance calculations. Note the excellent agreement in the reactance all the way down to about 800 Hz. It is not known what the cause of the deviation is below 800 Hz, but the two data are remarkably similar above this frequency. Furthermore, the resistance is in much better agreement than the smaller GTRI NIT. While these results are very encouraging, they raise questions about the efficacy of using relatively small impedance tube cross sectional areas to determine impedance. It is quite likely that the partial cell blockage that is inherent at the edges of the impedance tube plays a bigger role with smaller tube areas than with larger tube area. This question is left open until a more systematic study can be performed.

Grazing Incidence Tests

At grazing flows of M_{gr} = 0.00 and 0.30 in NASA's GIT, a broadband noise source and a series of 140 dB sinusoidal tones from 400 Hz to 3000 Hz were input. **Fig 21** shows the autospectra of the face sheet mic with no grazing flow, with grazing flow and the computed correlated autospectrum with grazing flow. The general character of the "speaker" source noise from M_{gr} = 0.00 and 0.30 is similar, however the flow spectra is only 3-4 dB higher than the no flow spectrum above 1000 Hz. Note that there is a very good signal-to-noise ratio. **Fig 22** shows the coherence between the LE face sheet mic and the reference face sheet mic near the middle of the liner span. The source is significantly correlated between the two face sheet microphones. **Fig 23** shows the in situ impedance computed with and without correlated autospectra. Because of the high signal-to-noise ratio (as evidenced by the high correlation seen in Fig 22), there is not a significant difference between impedance calculated with and without the 3-microphone noise rejection technique.

Fig 24 shows a comparison of the in situ impedance calculations and the educed impedance calculations with grazing flow of M = 0.3 and 140 dB tones. One can see good agreement above the resonance frequency (where the reactance crosses the x-axis) in the reactance, while there is not so good agreement in the resistance at these frequencies. Below resonance reveals a trend where the *in-situ* data exhibits what appears to be an anti-resonance behavior. It is not clearly understood why this "anti-resonance" behavior exists with the *in-situ* data, but not in the eduction technique. The main difference in the methodologies is that the *in-situ* method measures a local impedance while the eduction technique generates an average wall impedance over the entire treated section. Assuming the eduction method produces the realistic impedance (as it appears to based on normal incidence data), then installation of the instrumentation for the *in-situ* method may cause the discrepancy. For example, improperly sealed honeycomb and face sheet or honeycomb and back wall could alter the reactive liner assumption. However, the decision was made to move forward with the *in-situ* measurements planned for the full scale engine.

IV. Full Scale Engine Tests

The goal of this part of the program was to determine the liner surface impedance while it was installed on a static engine test stand. This section presents results from the *in-situ* acquisition of impedance of an installed liner on a Honeywell Tech7000 engine. Instrumentation from the normal impedance and grazing flow tests was installed

by Honeywell technicians into a liner that used the same face sheet as the laboratory tests, but with a honeycomb backing suitable for the inlet geometry.

A. Experimental Set-Up and Instrumentation of the Tech7000 Liner

Noise measurements were conducted at Honeywell's San Tan acoustic test facility. **Fig 25** shows the Honeywell Tech7000 engine installed on the test stand with an inflow control device (ICD). A polar array of 32 ground-plane microphones was used to collect the far field acoustic data. B&K 4134 microphones were placed in inverted stands that were spaced 0.275 inches above the ground on a 100-foot radius from the engine highlight. The microphones were positioned from 5 degrees to 160 degrees (relative to the engine inlet) in 5-degree increments, as indicated in **Fig 26.** Engine far field noise and internal inlet noise measurements were made with and without a barrier covering the exhaust of the engine. **Fig 27** is the measured far field noise at 30 degrees from the inlet centerline for the 75% N1C (Fan corrected speed) engine operating condition at 100 feet distance. The blade passage tone and its harmonics are clearly present in the measured noise spectrum. The design of a single-degree-of-freedom liners generally target this tone for noise reduction at critical engine noise certification conditions.

The inlet liner was instrumented in three locations near the fan face and three locations near the inlet entrance. **Fig 28** shows the instrumented treatment prior to final installation in the inlet nacelle. There are six locations in the inlet where a face sheet sensor and a backing cavity sensor were placed in the treatment within a given honeycomb cell. The 2 axial locations and 3 circumferential locations are depicted in **Fig 29**.

B. Engine Inlet Test Conditions

The engine was run at a range of engine power settings. Data was acquired at 48%, 54%, 60%, 75%, 82%, and 91% engine power. The grazing flow Mach number near the fan face was estimated to be between 0.2 and 0.4 from the lowest to the highest engine power setting, respectively.

C. Adjustments to Impedance Measurements

A correction was made to the liner impedance based on known changes to the perforate geometry. Specifically, the face sheet microphone replaced an orifice hole that would ordinarily be open over a given honeycomb cell. This effectively reduced the local porosity and hence local impedance of the liner. The microphone tube also reduced the honeycomb cell volume to a lesser extent. The effect of the instrumentation replacing an orifice hole was demonstrated clearly in the initial normal incidence impedance tube results presented earlier (see Fig 12). As expected the local impedance, and particularly the local resistance, is increased when the microphone replaces an orifice hole. Almost all of the resistance resides in the face sheet which is directly proportional to the porosity under relatively moderate sound pressure levels. The reactance consists of the mass reactance (the reactance due to the face sheet porosity) and the cavity reactance (due to the honeycomb cell volume). Reducing the porosity tends to shift the liner resonance (where the normalized reactance is zero) to a lower frequency whereas reducing the volume tends to increase this frequency. The two effects work against each other. In the present case, the overall effect is not large. The estimated percent change in cell volume due to the presence of the microphone is approximately 12%. The estimated change in perforate hole area is about 16%. Since these parameters have opposite effects on the resonant frequency (the reactance), little change is expected in the reactance due to the presence of the microphone. This can be seen in **Fig 12**.

The estimated average porosity covering a honeycomb cell (assuming 6 perforate holes over a given cell on average) is 12.5%. With a microphone installed in place of an orifice, this estimated porosity is 10.4%. Thus, the measured resistance using Dean's method will be artificially higher than what exists over the rest of the un-instrumented liner. The data can therefore be corrected by reducing the measured resistance by a ratio of the porosity differences.

D. Results

Data from the test *Configuration #31* at San Tan was processed and the *in-situ* impedance was calculated for several liner locations for several engine speeds. There were 6 pairs of sensors (backing cavity and face sheet) with 3 pairs located at an axial station near the inlet entrance and 3 pairs located at an axial station near the fan face. The sensor pairs were located at the 2 o'clock, 5 o'clock, or 10 o'clock position around the inlet barrel (see **Fig 29**). Initial investigation of the sensor spectral results suggest that the 5 o'clock transducer at the fan face axial location and the 10 o'clock transducer at the inlet entrance location did not record valid data.

GTRI developed a Labview-based program that takes the raw engine test file and computes the FFT for the pertinent channels. The processing produced auto spectra, phase, cross spectra, and coherence for all microphone combinations with an 8 Hz bandwidth and over 700 ensemble averages. Then a MatLab code was written to take the relevant results and compute the local surface impedance via Dean's method. These programs have been provided to Honeywell so all raw data can be processed as needed.

Impedance Measurements from Static Engine Test

Typical auto spectra from face sheet microphones and their corresponding back wall microphones are shown in **Fig 30a and Fig 30b** for the fan face and inlet entrance locations, respectively. Phase differences measured between the face sheet and back wall microphones are shown in **Fig 31a and Fig 31b.** Note that the phase for the 5 o'clock location at the fan face axial location and the 10 o'clock location at the inlet entrance location are clearly outliers. Thus, data from the 5 o'clock fan face and 10 o'clock inlet entrance locations are not presented due to spurious results. Using the remainder of these data to compute impedance (with no correction for the face sheet and no signal enhancement) results in the resistance and reactance shown in **Fig 32**.

An initial check of the data using the signal enhancement technique is shown in **Fig 33** where impedance computed from engine data are shown along with the GTRI's normal impedance results (from 1.13" diameter tube) using engine liner samples of comparable thickness. Note that the data resulting from the signal enhancement technique is sparse in some areas. This is because a coherence limit was imposed (here 0.01) below which data points were thrown out. A clear trend is still observed in the data however. Very good agreement was found between the normal incidence impedance tube data at GTRI and the grazing flow impedance calculated from the engine data at this low power setting.

The impedance results computed from engine runs show expected trends with resistance and reactance and indicate a liner resonance frequency near 2700 Hz very close to the liner design intent with normalized resistance near 1.5.

Employing the 3-microphone flow noise separation technique was successful in determining the impedance at the higher engine power settings where it was found that using a more stringent coherence limit produced more accurate results in the reactance calculations **Fig 34** shows the resistance and reactance as estimated by the *in-situ* impedance method for two engine power settings. Minimal changes in these parameters are expected of the linear liner. A slight change in reactance was observed with Mach number in the NASA GIT data.

Fig 35 shows a comparison between configuration #31 and #32 for the lowest power setting at the 2 o'clock fan face location. **Fig 36** shows data for the same conditions at the 10 o'clock fan face location. Note that in these two cases, no flow rejection methodology is employed. The agreement is excellent and this offers a good example of data repeatability. **Fig 37** shows the same results at the *fan face* location except the 3 microphone flow rejection technique is employed. **Fig 38** shows results at the *inlet entrance* location at the 5 o'clock location instead of the 10 o'clock location.

Figs 39a-c show the data at the fan face 2 o'clock position for 75%, 82% and 91% engine power settings respectively. The 75% and 82% data used a coherence criteria limit of 0.01 while the 91% data used a criterion of 0.3. It appears the scatter in the 75% and 82% data can be reduced by making the criterion 0.3 as well. Also note that repeatability in the experiments is excellent as data from engine configuration #31 and #32 are shown.

Finally, **Fig 40** shows vividly how the flow rejection technique can help in the impedance calculations. If this technique is not used, the computed impedance can be very inaccurate at frequencies that do not have good signal-to-noise ratios. As an example, two frequencies can be examined at a condition where the flow noise will be most severe, namely the 91% engine power setting. The blade passing frequency (BPF) at 91% power is 3320 Hz (see **Fig 41**) at the 2 o'clock face sheet microphone location. Many other high amplitude tones are present in the spectra that are harmonics and rotor-stator interactions. In-between these tones, a certain level of broadband noise exists and a frequency in-between tones like 912 Hz can be used for comparison. Both the broadband noise and some of the other tones present have lower signal-to-noise (S/N) levels than the large BPF tone, so one expects that the coherent signal processing technique used here to be a significant enhancement on the former noise rather than on the BPF tone. We can show this by examining the computed resistance and reactance with and without the 3-mic technique at a high S/N case and a low S/N case. The table below summarizes this comparison.

Data from 2 o'clock Fan Face Location

		No 3-Mic Technique 91% Engine Power		With 3-Mic Technique 91% Engine Power		With 3-Mic Technique 48% Engine Power	
Frequency (Hz)	S/N	R/ρc	X/ρc	R/ρc	X/ρc	R/ρc	X/ρc
3320	High	2.32	-0.36	2.32	-0.36	1.61	0.32
912	Low	2.82	-5.73	2.28	-4.62	1.58	-4.62

Table 1. Effect of 3-mic coherence technique on impedance calculation for low S/N

Unfortunately, the published normal incidence data from Honeywell doesn't include data below 1500 Hz, but the data at the lowest engine setting (48% power) can be used as a guide. The BPF at 3320 Hz is an example of a high S/N case and the noise at 912 Hz is an example of a low S/N case. Note that at the high S/N case, the 3 microphone technique has no affect on the impedance calculation. If these values are compared to the 48% power case, one can see that the coherence technique helps to compute a more accurate impedance. The reader should note that the large reduction in the resistance between the 91% power and 48% power setting can be attributed to the sound pressure level and grazing flow differences.

Using coherent source data improves the signal-to-noise dramatically. In the fan face plane, the 2 o'clock sensor pair uses the 10 o'clock face sheet sensor for correlating, and the 10 o'clock sensor pair uses the 2 o'clock face sheet sensor for correlating. This was done since we don't have good faith in the 5 o'clock sensors (although the face sheet sensor might be okay). In the inlet entrance plane, the 2 o'clock sensor pair uses the 5 o'clock face sheet sensor and vice versa. The 10 o'clock face sheet sensor was not used for the same reason the 5 o'clock fan face sensor was not used.

In general, the data is consistent from configuration #31 (no barrier) to #32 (barrier covering the exhaust) with regard to repeatability. General observations are:

1) The liner acoustic impedance has been successfully measured on an engine at 4 different locations (Successful defined as validated by impedance tube measurements). Expected trends with increasing grazing flow were observed.

2) The 3-microphone coherence-based flow rejection technique has been successfully applied to the data and is necessary at the high power settings to accurately educe the impedance with the *in-situ* method.

3) Data acquired near the inlet entrance exhibits more scatter, most likely due to increased grazing flow velocity compared to the fan face location.

4) A larger coherence limit criterion, in the 3-mic processing, was used at the higher engine power settings to get smoother results.

5) Good repeatability was observed between configuration #31 and #32

Further Analysis of Data

The liner impedance data gathered from the engine test is examined further in conjunction with earlier impedance work performed at GTRI using a similar liner face sheet (~10 Rayl screen with a ~13% open area and 0.032" thick perforate). The measured resistance from the engine test has been compared to both the resistance measured in the GTRI impedance tube and GTRI's DC flow tube. This has shed additional light on the consistency of the engine data.

There are three things that will affect the acoustic resistance of the face sheet: 1) The incident sound pressure level, 2) The grazing flow velocity, and 3) the local increase in resistance due to the presence of the pressure instrumentation taking the place of a perforate hole in the face sheet. All three of these effects are present in the engine data. Increased engine power increases the grazing flow and the SPL of the incident sound on the liner.

The first two can be simulated in an impedance tube and a DC flow tube. The last effect can be accounted for by processing the data to reflect a lower resistance than measured by virtue of the ratio of local face sheet porosity with and without instrumentation. All data presented previously accounts for this by decreasing the resistance by a factor of (10.4/12.5) which is the porosity ratio of an average cell with 5 exposed perforate holes to one with 6 exposed holes.

The effect of instrumentation placement is shown in **Fig 42** (see also Fig 12) where, as expected, the resistance of the face sheet is increased with the face sheet porosity reduced by the instrumentation. **Fig 43** shows how incident

SPL affects the acoustic impedance measured with the *in-situ* method in GTRI's impedance tube. The increased particle velocity due to the increased SPL results in an increase in acoustic resistance.

For plane wave propagation (not true in the engine environment), the incident particle velocity can be estimated from the sound pressure level measured from the flush-mounted microphone on the face sheet. If we examine the liner resonance condition (i.e., when the reactance goes to zero), and assume that the impedance of the face sheet is dominated by the resistance, then the particle velocity at the face sheet can be estimated as:

$$u_{rms} \approx \left. \frac{P_{rms}}{R} \right)_{@\,\text{liner resonance}} \tag{6}$$

Here, R is the normalized specific acoustic resistance. Using a value of $1.75\rho c$ for R and the P_{rms} that corresponds to 145 and 155 dB, the incident particle velocity is estimated to be 50 cm/s and 155 cm/s, respectively.

Fig 44 shows DC flow tube data showing the normalized resistance as a function of incident velocity. Corresponding SPL points are shown to identify relative particle velocities. The range of DC resistance between approximately 50 and 155 cm/s is in the range of measured acoustic resistance in the impedance tube.

Fig 45 shows several data sets of the liner face sheet resistance. Engine data at a high and lower engine power setting is compared with impedance tube data (using both TMM and *in-situ* techniques). The TMM reveals an anti-resonance that is not present *in-situ* technique and shows a resistance that may be affected. At the system resonance (around 2650 Hz), the measured resistance using the TMM should be most accurate and indeed, it is in excellent agreement with the *in-situ* data.

V. Summary and Conclusions

Results of this joint Honeywell/GTRI/NASA effort have demonstrated that it is possible to measure local liner impedance in an engine fan duct, *in situ*, with a reasonable degree of accuracy. This was accomplished by comparison of engine measured impedance data with both quiescent impedance tube and grazing flow duct impedance measurements.

The objective for these *in-situ* measurements is to substantiate treatment design, provide understanding of flow effects on installed liner performance, and provide modeling input for fan noise propagation computations. In addition, a great deal of practical experience was gained in dealing with instrumentation installation that was critical to the success of this measurement technique. These "lessons learned" have been documented in this report.

Furthermore, it was demonstrated that higher fidelity results can be obtained by using a three-microphone coherence technique that can enhance signal-to-noise ratio at high engine power settings. This was clearly demonstrated at the higher engine power settings where the grazing flow velocity was the highest. A suitable correction can be applied to obtain an impedance that reflects an average impedance unaffected by the local instrumentation.

Acknowledgments

This work was funded under NASA Contract NAS3-00136 from the NASA Glenn Research Center. The encouragement and support of Joe Grady, NASA Program Manager, is appreciated. Special thanks to Honeywell for their program leadership, technical guidance, and engine test results under the Engine Validation of Noise and Emissions Reduction Technology (EVNERT) program. Many of the experiments at GTRI and NASA were performed with the help of Georgia Tech undergraduate coop students from the School of Aerospace Engineering. The authors would like to thank Robert Combier, Nathanial Hunter, and Adam Churney of Georgia Tech and Brian Howerton and Carol Harrison of NASA LaRC for their work on this project. Finally, the work of PhD candidate Don Nance regarding implementation of the three-microphone coherence method was appreciated.

References

[1]Guess, A. W. "Calculation of Perforated Plate Liner Parameters from Specified Acoustic Resistance and Reactance" *Journal of Sound and Vibration*, Vol. 40 No. 1, 1975

[2]Dean, P. D. "An *In-Situ* Method of Wall Acoustic Impedance Measurement in Flow Duct" *Journal of Sound and Vibration*, No. 34 (1), 1974

[3]Hubbard, et al editor *Aeroacoustics of Flight Vehicles: Theory and Practice Vol I. and Vol II* NASA reference publication, 1995.

[4]ASTM E1050-98 Standard Test Method for Impedande and Absorption on Acoustical Materials Using A Tube, Two Microphones and a Digital Frequency Analysis System .

[5]Chung, J. Y. and Blaser, D. A. *Transfer Function Method of Measuring In-Duct Acoustic Properties: I. Theory* Journal of the Acoustical Society of America, Volume 68, No. 3, Sept., 1980.

[6]Mechel, F. Pl, Mertens, P.A. and Schilz, M. Interaction between Air Flow and Airborne Sound in a Duct *AMRL-TR-69-53*, 1969.

[7]Feder, E. and Dean, L. W. *Analytical and Experimental Studies for Predicting Noise Attenuation in Acoustically Treated Ducts for Turbofan Engines* *NASA Contractor Report CR-1373* September, 1969.

[8]Rao, K., and Munjal, M. *Experimental Evaluation of Impedance of Perforates with Grazing Flow* Journal of Sound and Vibration, Vol. 108, No. 2, 1986.

[9]Hersh, A. and Walker, B. *Acoustic Behavior of Helmholtz Resonators, Part II: Effects of Grazing Flow* CEAS/AIAA Paper 95-079, Presented at the 16th Aeroacoustics Conference, Munich, Germany, 1995.

[10]Kraft, R. E. *Theory and Measurement of Acoustic Wave Propagation in Multi-Segmented Rectangular Flow Ducts* PhD Thesis, University of Cincinnati, 1976.

[11]Mariano, S., Bohn, N., Russel, P., Schnell, A. and Parsons, G. A Study of the Suppression of Combustion Oscillations with Mechanical Damping Devices *NASA CR90094*, 1967.

[12]Dean, P. D. "An *In-Situ* Method of Wall Acoustic Impedance Measurement in Flow Duct" *Journal of Sound and Vibration*, No. 34 (1), 1974.

[13]Phillips, B. Effects of High Wave Amplitude and Mean Flow on a Helmholtz Resonator NASA TM X-1542.

[14]Binek,J. M.Sc. Dissertation, Institute of Sound and Vibration Research, University of Southampton, Behavior of Acoustic Resistance of Typical Duct Liners in the Presence of Grazing Flow Measured by a Two Microphone Method

[15]Murray, P., Ferrante, P. and Scofano, A. "Manufacturing Process and Boundary Layer Influences on Perforate Liner Impedance" AIAA-2005-2849 11th AIAA/CEAS Aeroacoustics Conference, Monterey, CA 23-25 May 2005.

[16]Zandbergen, T., Laan, J. N., Zeemans, H.J., and Sarin, S. L. "In-Flight Acoustic Measurements in the Engine Intake of a Fokker F28 Aircraft" AIAA-83-0677 8th AIAA Aeroacoustics Conference, Atlanta, GA 11-13 April 1983.

[17]Zandbergen, T.. "On the Practical Use of Three-Microphone Techniqe for *In-Situ* Acoustic Impedance Measurements on Double Layer Flow Duct Liners" AIAA-81-2000 7th AIAA Aeroacoustics Conference, Palo Alto, CA 5-7 October, 1981.

[18]Watson, W. Jones, M., Tanner, S. and Parrott, T "Validation of a Numerical Method for Extracting Liner Impedance" *AIAA Journal* vol. 34, No. 3, March 1996, pp548-554.

[19]Nance, D and Ahjuja, K. K. , T.. "Limitations of the Three-Microphone Signal Enhancement Technique" AIAA-2007-441 45th AIAA Aerospace Sciences Conference, Reno, NV, 8-11 January 2007.

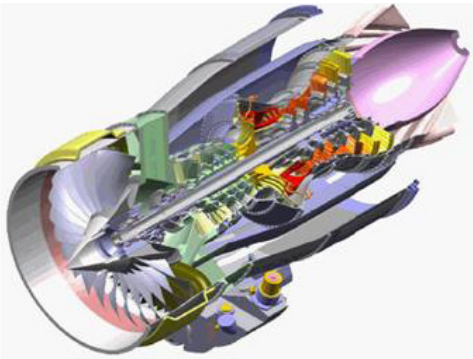

Fig 1. Cutaway drawing of Honeywell's Tech7000 engine.

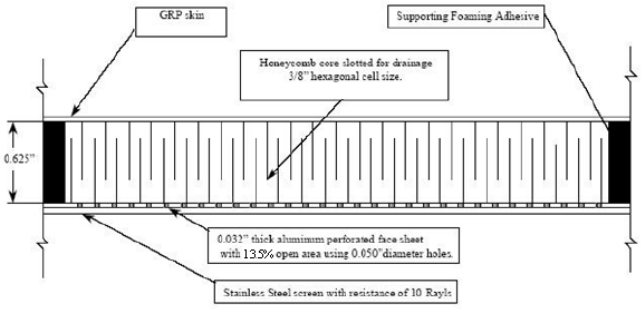

Fig 3. Liner acoustic lining system in inlet of Tech7000 nacelle.

Parameter	Tech7000
Takeoff Thrust	7000 lb to ISA+15C
Cruise Thrust (ISA, 35K, 0.7M, Installed)	Rated to 1,910 lb
TSFC (Min Engine) (Cruise Flight)	0.642 lb/hr/lb
Fan Diameter	34.2 in
Weight	1364 lb
Thrust to Weight	1.40
Engine Length	73 in
Pressure Ratio	28.7

Table 1. Honeywell's Tech7000.

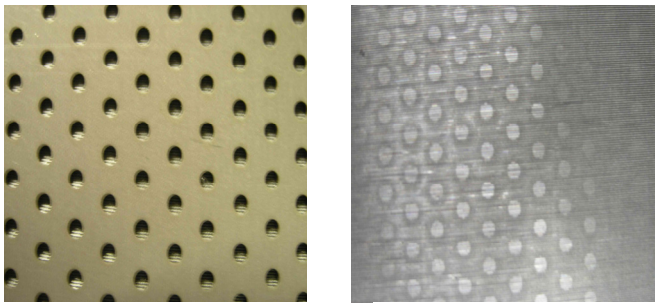

a) perforate side b) wire mesh side

Fig 4. Face sheet used for EVNERT liner tests. a) perforate side, b) wire mesh side (flow/source side).

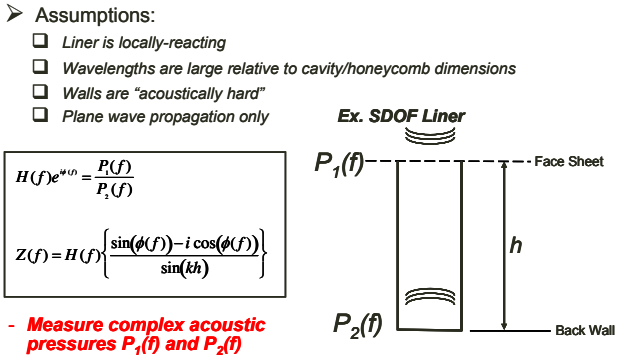

Fig 2. Dean's two microphone in-situ method for impedance determination for a single degree-of-freedom resonant liner.

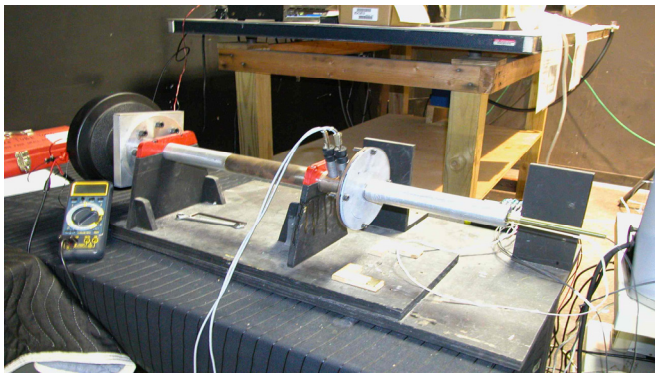

Fig 5. GTRI normal incidence impedance tube; 1.12-inch diameter.

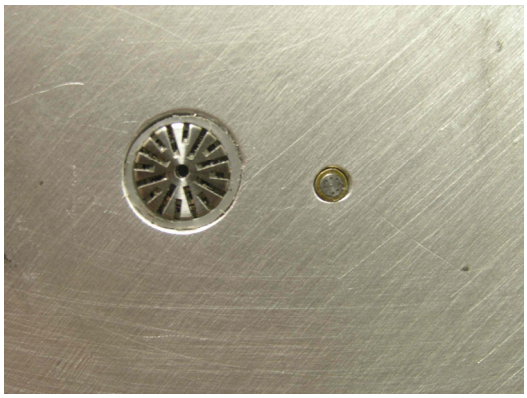

Fig 6. Endevco calibration set-up: B&K ¼-inch reference.

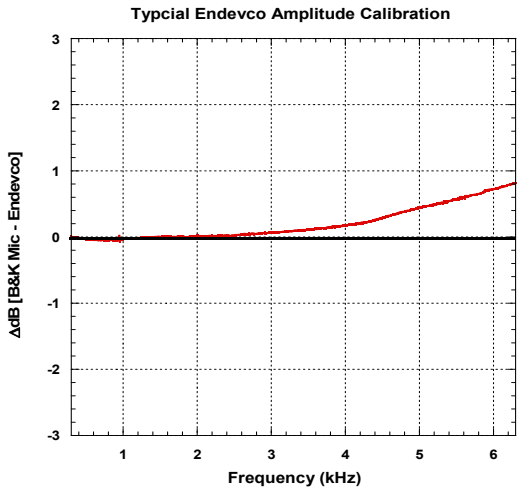

Fig 9. Measured amplitude differences between Endevco mics referenced to B&K mic.

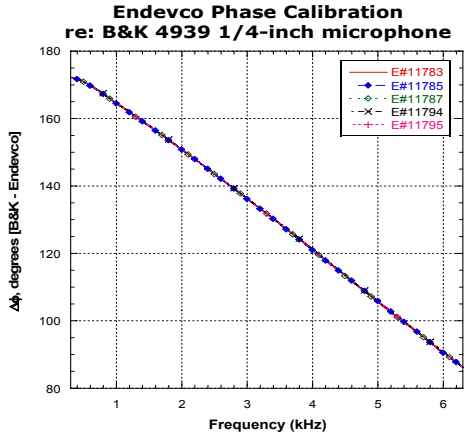

Fig 7. Phase relationship between Endevco mics referenced to B&K mic.

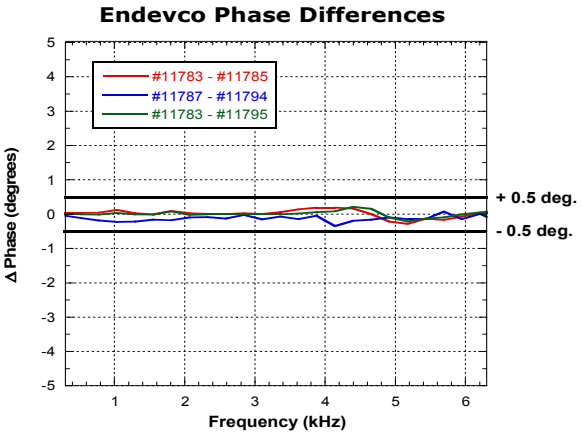

Fig 8. Measured phase differences between Endevco mics.

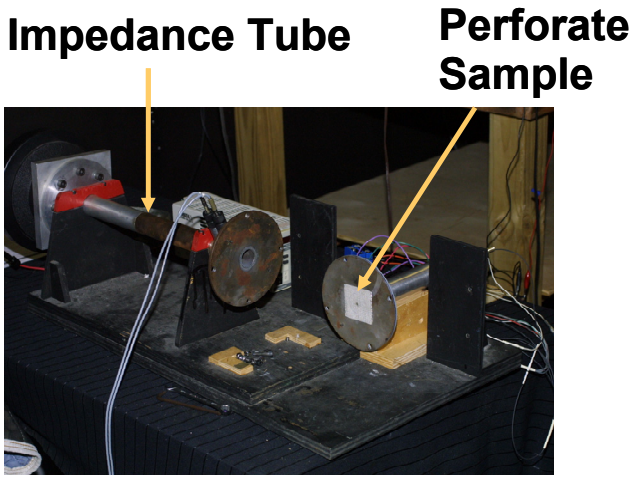

Fig 10. Liner perforate tested in GTRI normal incidence impedance tube.

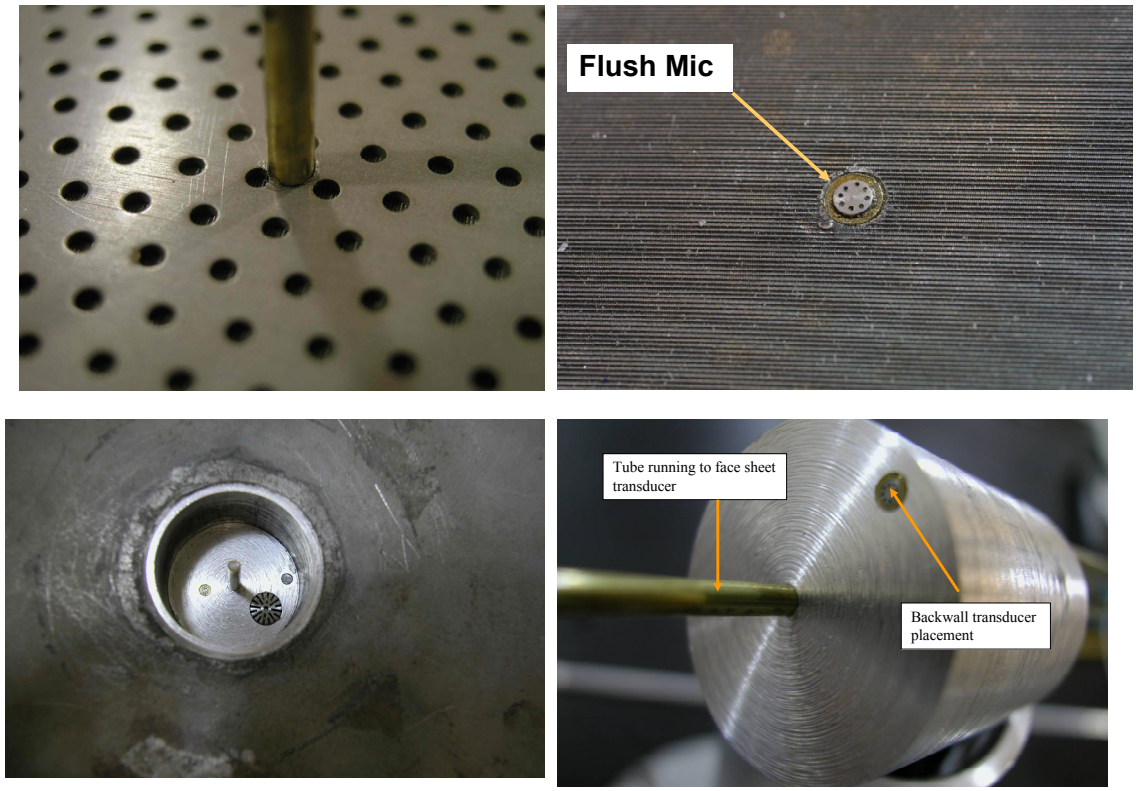

Fig 11. *In situ* mic installation for impedance tube measurements.

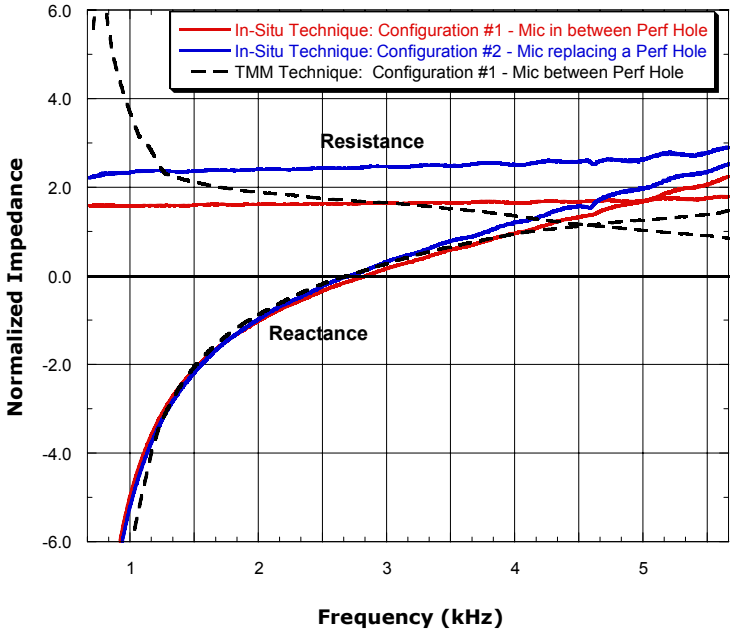

Fig 12. Effect of face sheet microphone location; note increased resistance with face sheet microphone replacing perforate hole.

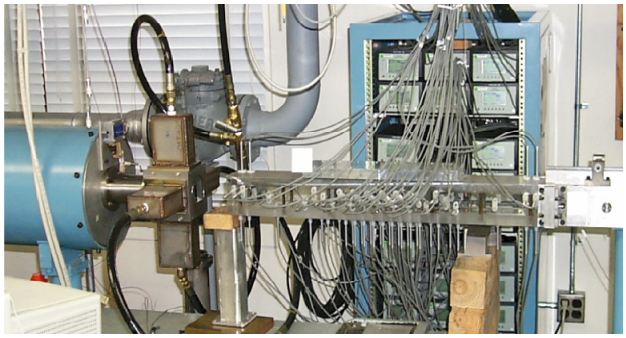

Fig 13. NASA's Grazing Incidence Tube.

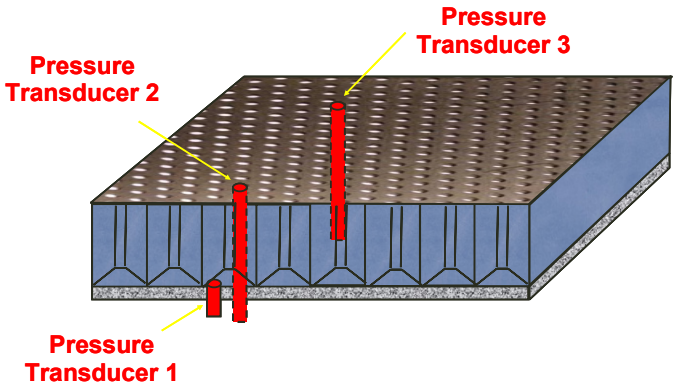

Fig 14. Application of 3-Microphone signal enhancement technique to in situ measurements.

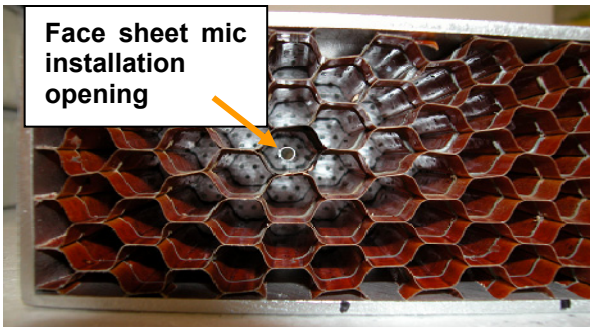

Fig 15. NASA GIT entry 1 test liner; back side looking forward.

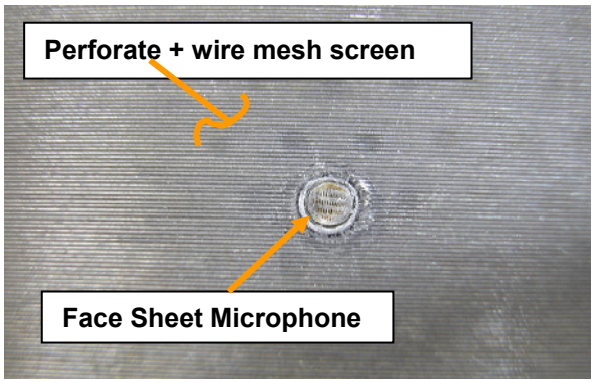

Fig 16. Typical face sheet microphone installation.

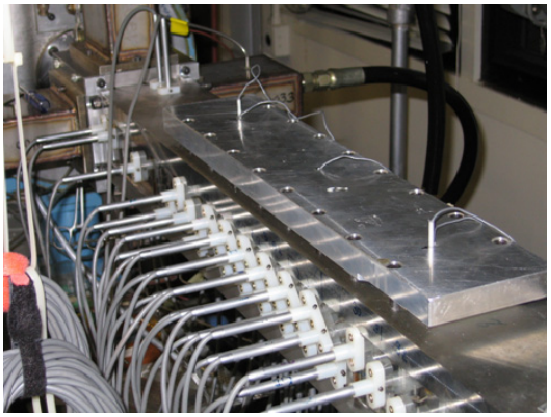

Fig 17. Test liner installed in NASA's GIT.

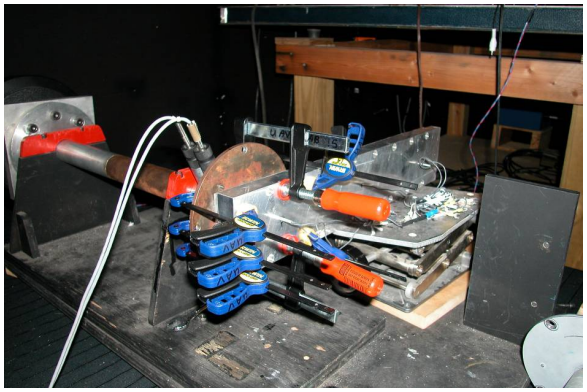

Fig 18. Grazing flow test liner installed on GTRI small impedance tube.

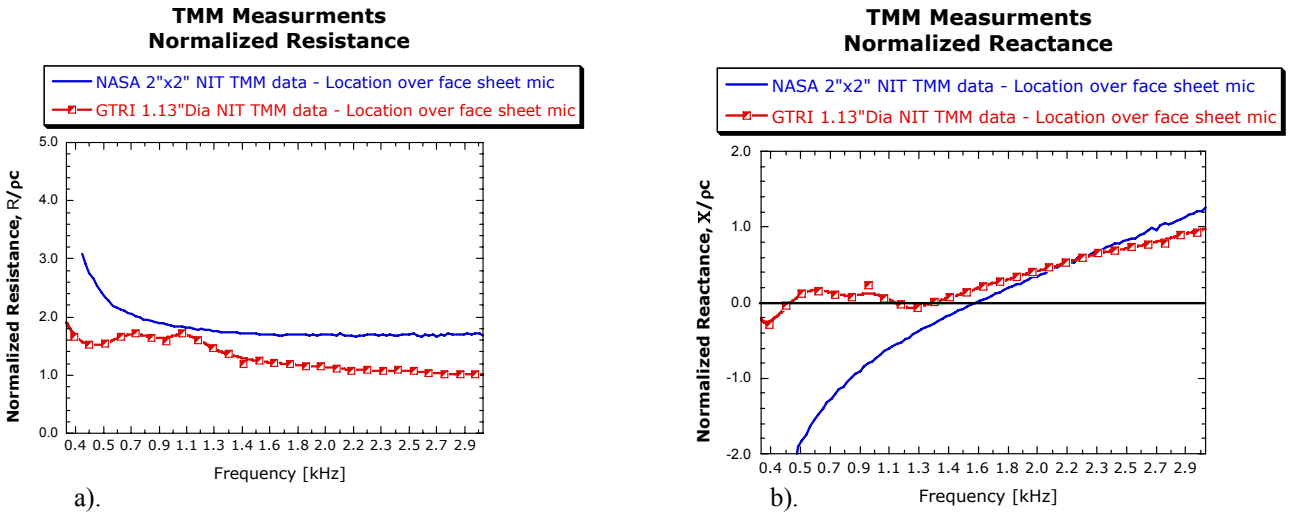

a). b).

Fig 19. Comparison of normal incidence impedance of refurbished test liner: NASA 2"x2" NIT vs. GTRI 1.13" Dia NIT.

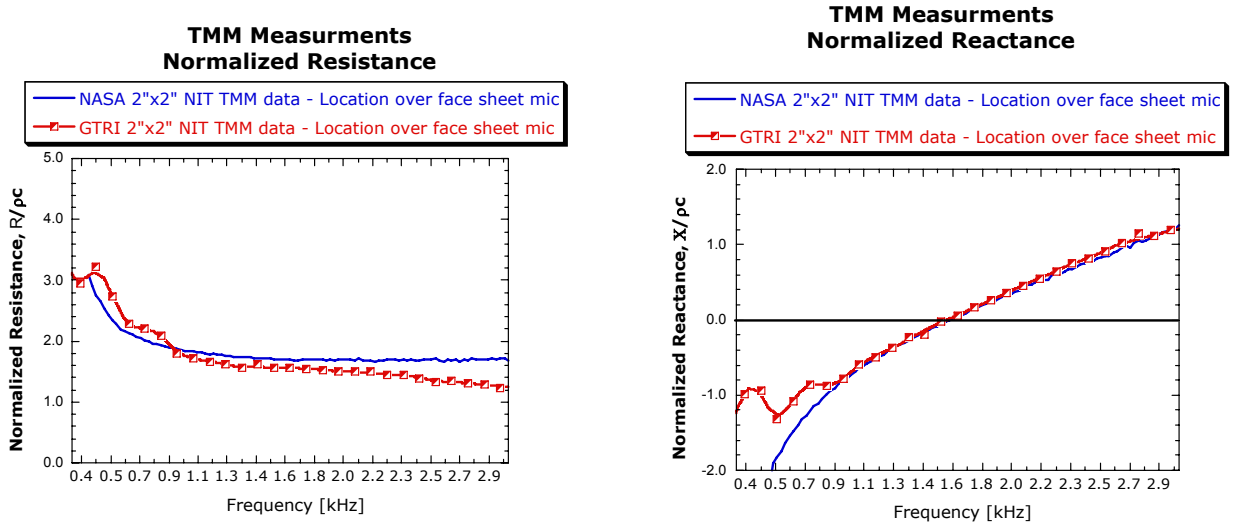

a). b).

Fig 20. Comparison of normal incidence impedance of refurbished test liner: NASA 2"x2" NIT vs. GTRI 2"x2" NIT.

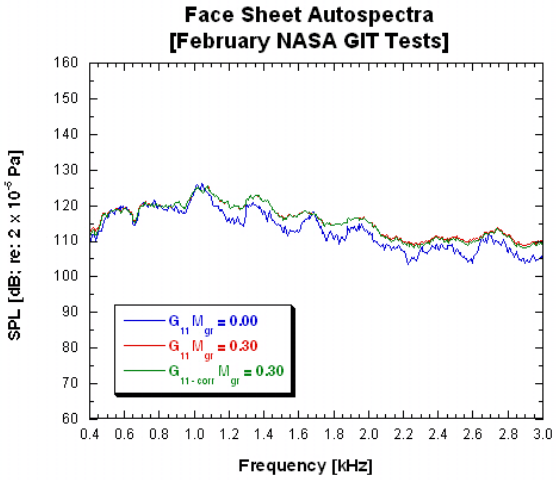

Fig 21. Correlated and uncorrelated SPL spectra of LE face sheet microphone.

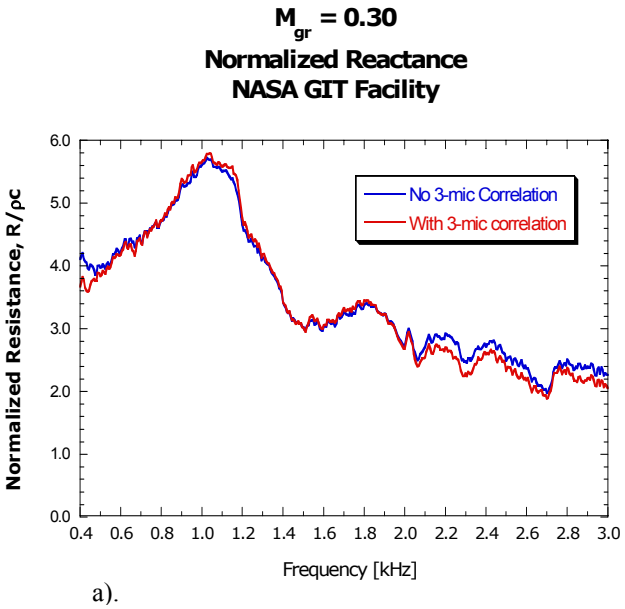

a).

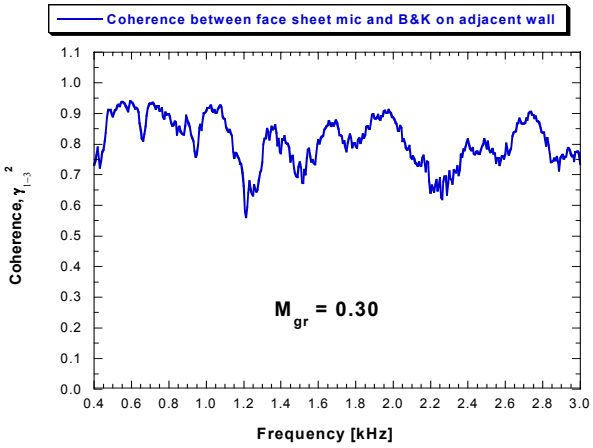

Fig 22. Coherence between LE face sheet mic and reference face sheet mic.

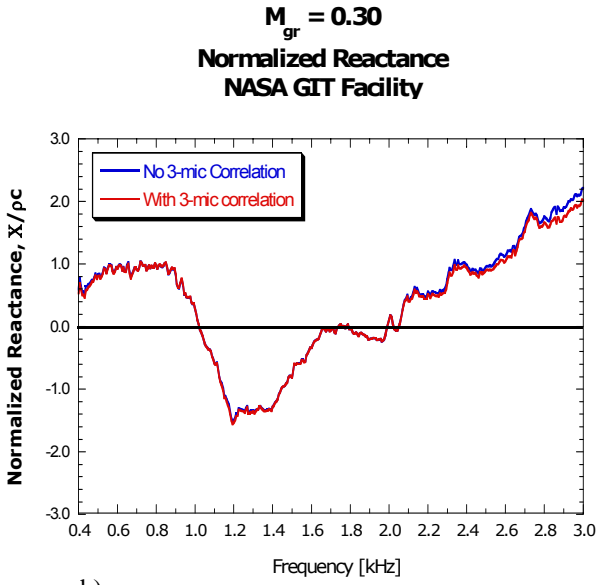

b).

Fig 23. Comparison of in-situ impedance computed with and without 3-mic correlation.

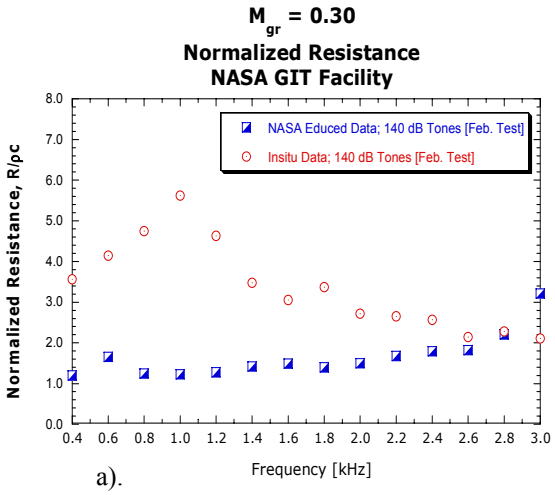

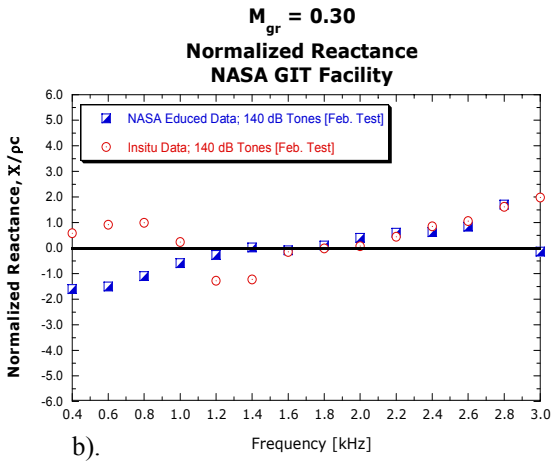

Fig 24. Comparison of in situ and educed data from NASA GIT [Feb. test], M_{gr} = 0.30; 140 dB tone source.

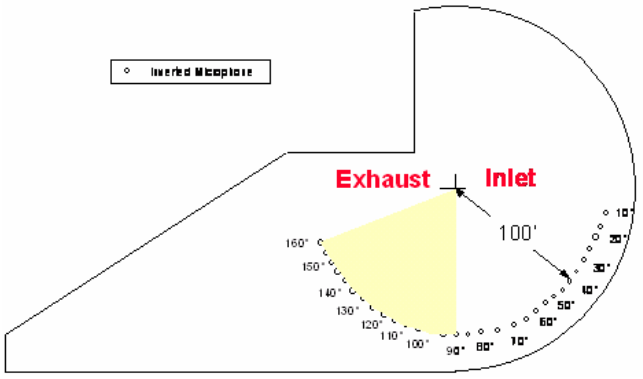

Fig 26. Far field microphone array at San Tan.

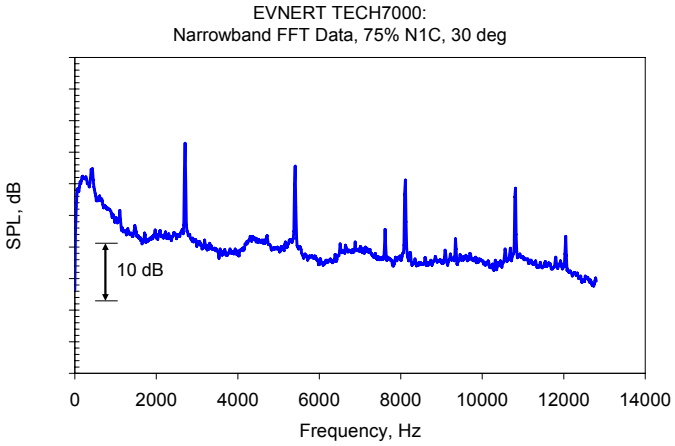

Fig 27. Narrowband far field noise spectrum at 30°.

Fig 25. Engine support structure is designed for minimum acoustic and inflow interference.

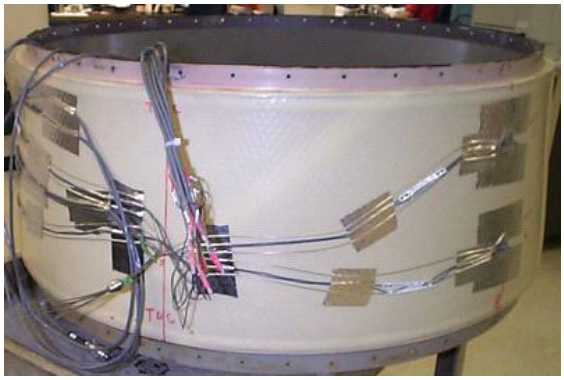

Fig 28. Instrumentation of inlet nacelle and schematic of sensor locations in the inlet for *in-situ* impedance engine testing.

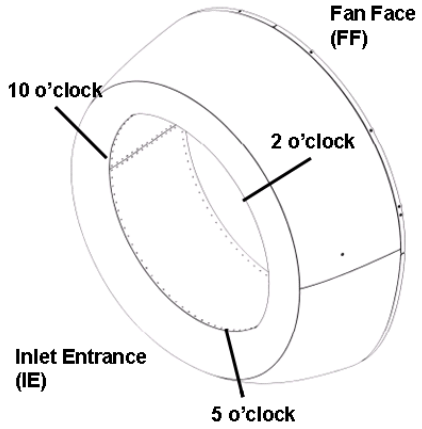

Fig 29. Instrumentation of inlet nacelle and schematic of sensor locations in the inlet for *in-situ* impedance engine testing.

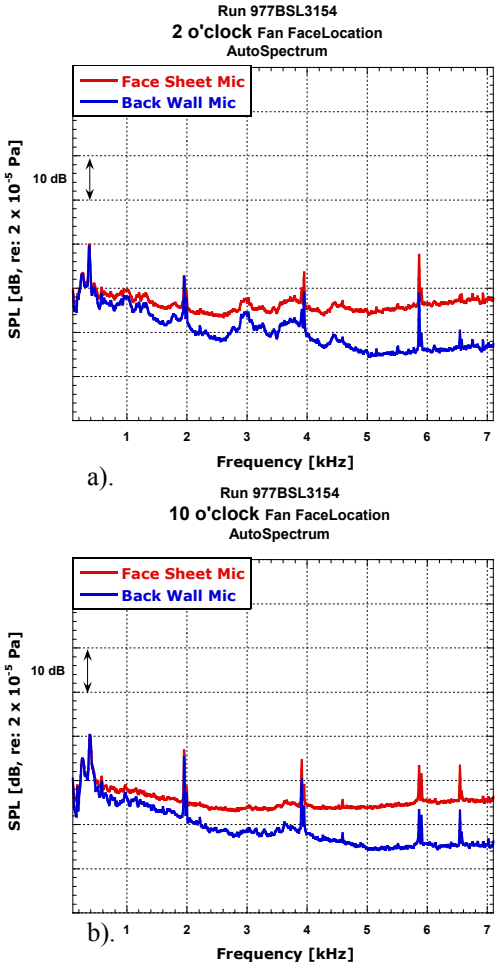

Fig 30. Face sheet and backwall spectra from 2 o'clock locations at the a) fan inlet and b) inlet entrance positions.

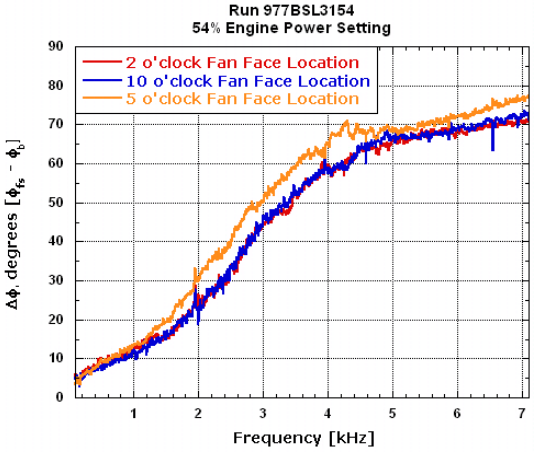

a). Three liner locations at the fan face at 54% engine power. Note the deviation of the 5 o'clock location from the other two.

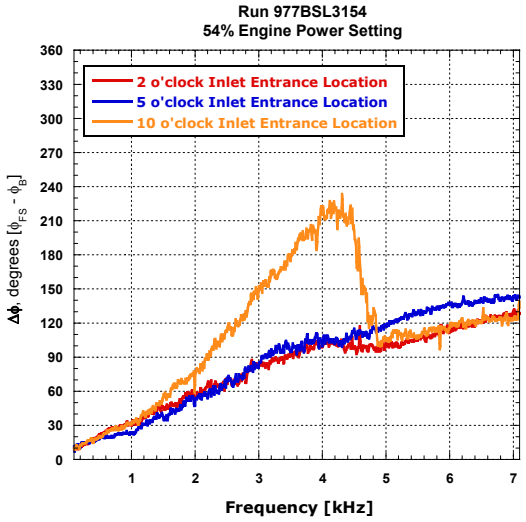

b). Three liner inlet entrance locations at 54% engine power. Note the deviation of the 10 o'clock location from the other two.

Fig 31. Typical measured phase between face sheet and back wall microphones.

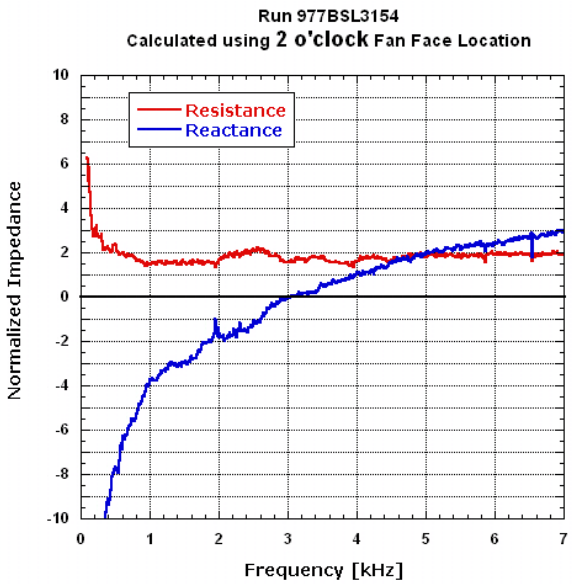

a). 2 o'clock fan face location.

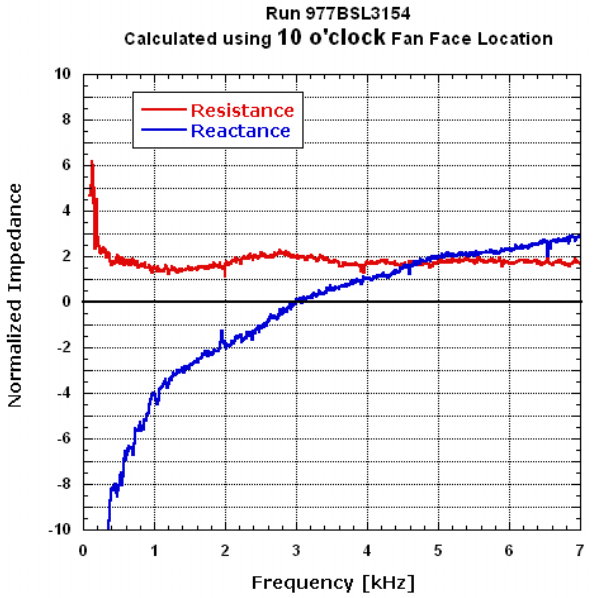

b). 10 o'clock fan face location.

Fig 32. Calculated impedance using data from 2 and 10 o'clock fan face location. No signal enhancement or face sheet correction is applied, engine power is 54%.

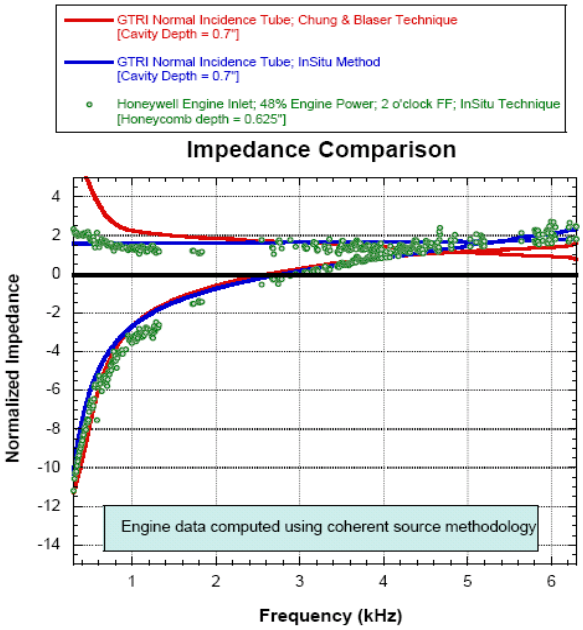

Fig 33. Impedance Comparison of Engine Inlet Impedance at 48% Power with GTRI Normal Incidence Tube Results using the *In-situ* Method and the Standard 2-Mic Method.

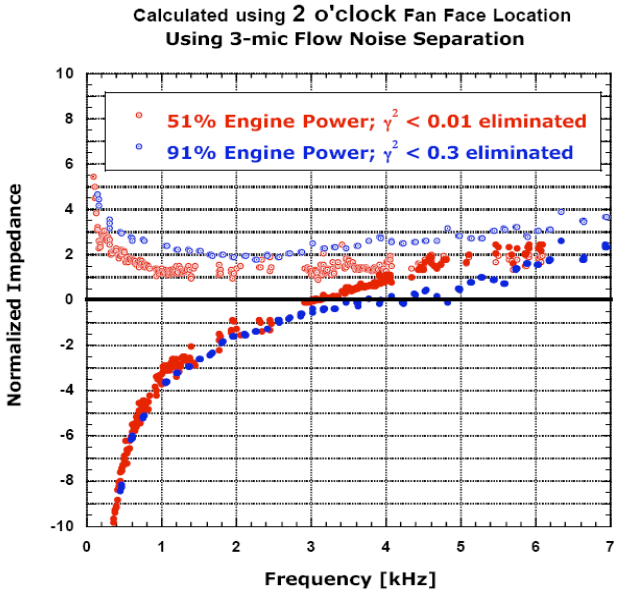

Fig 34. Resistance and Reactance at Low and High Engine Power Settings using the In-situ Impedance Method.

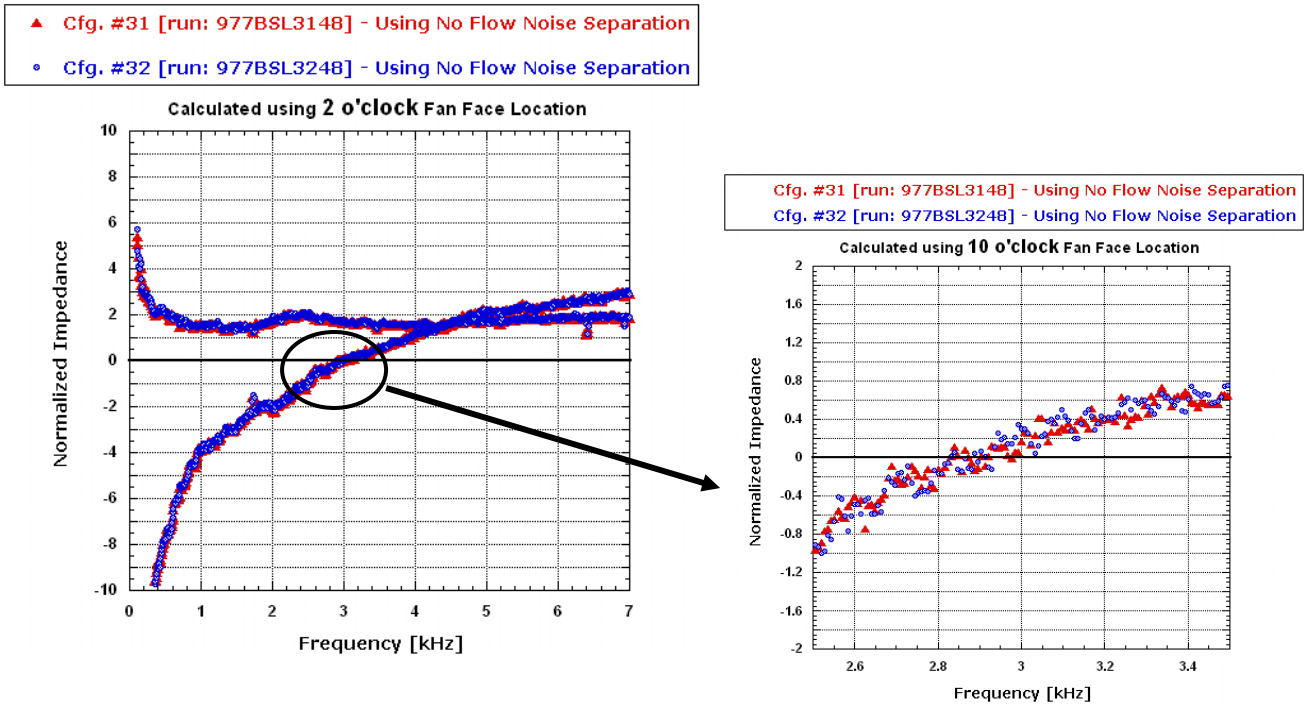

Fig 35. Comparison of Engine Test Configuration on Computed In-situ Impedance. Engine Power: 48%, Fan Face Location, 2 o'clock Location; No Flow Noise Rejection.

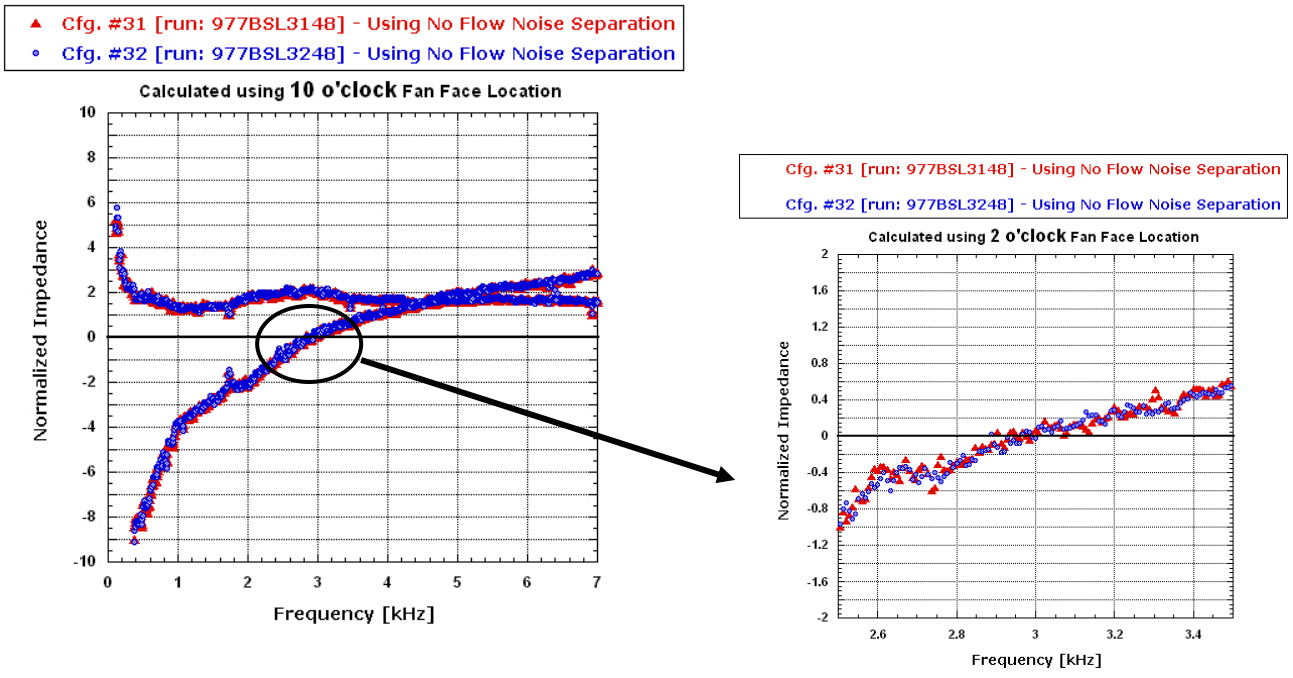

Fig 36. Comparison of Engine Test Configuration on Computed In-situ Impedance. Engine Power: 48%, Fan Face Location, 10 o'clock Location; No Flow Noise Rejection.

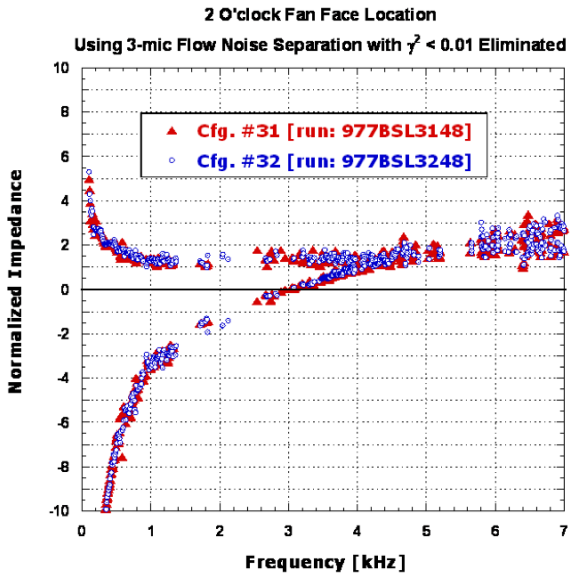

a). 2 o'clock fan face location.

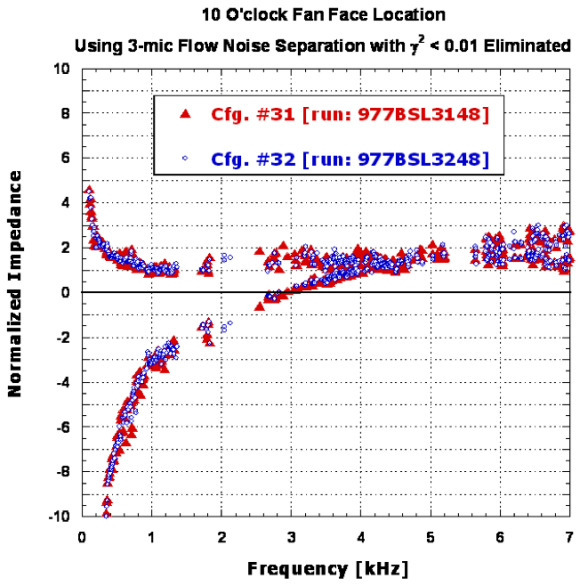

b). 10 o'clock fan face location.

Fig 37. Comparison of Engine Test Configuration on Computed In-situ Impedance. Engine Power: 48%, Fan Face Location, 2 and 10 o'clock Location; with 3-Mic Flow Rejection.

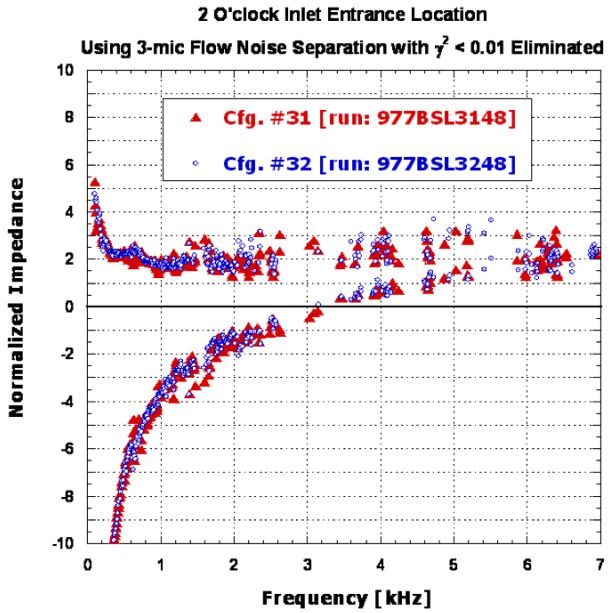

a). 2 o'clock inlet entrance location.

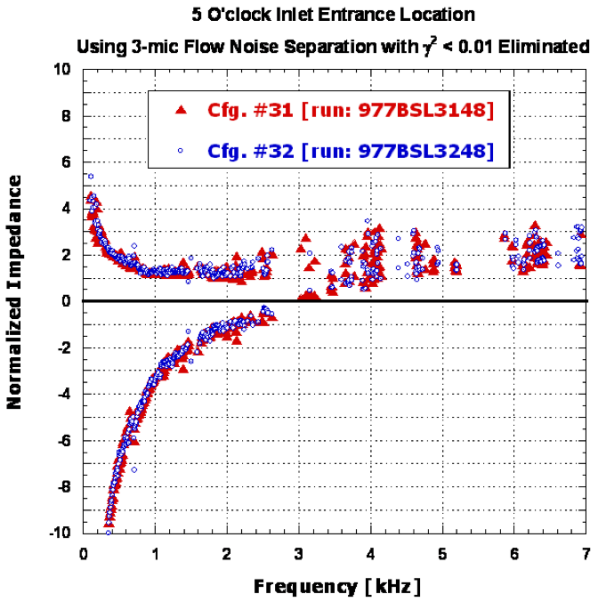

b). 10 o'clock inlet entrance location.

Fig 38. Comparison of Engine Test Configuration on Computed In-situ Impedance. Engine Power: 48%, Inlet Entrance Location, 2 and 5 o'clock Location; with 3-Mic Flow Rejection.

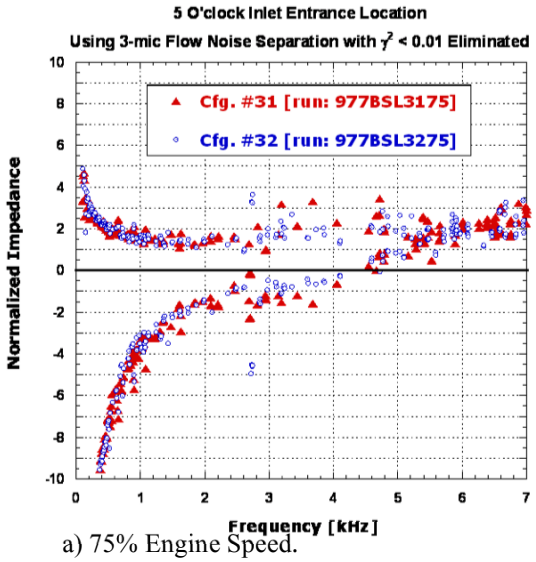

a) 75% Engine Speed.

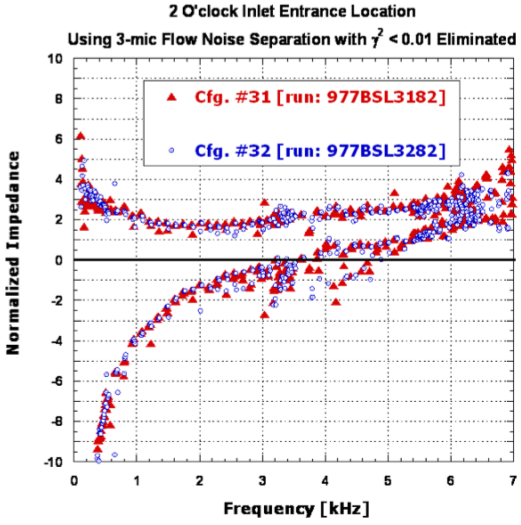

b) 82% Engine Speed.

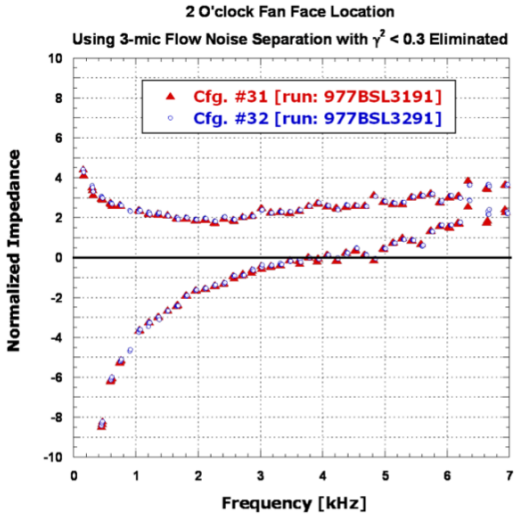

c) 91% Engine Speed.

Fig 39. Comparison of Engine Test Configuration on Computed In-situ Impedance. Engine Power Settings: 75%, 82%, and 91%; Fan Face location, 2 o'clock Location; with 3-Mic Flow Rejection.

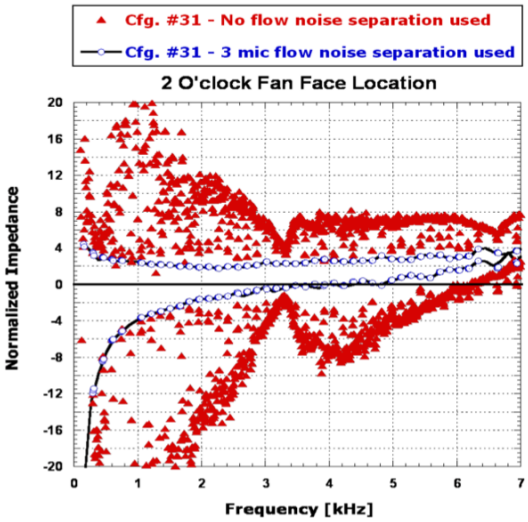

Fig 40. In-situ Impedance Comparison with and without Flow Noise Rejection. Engine Power: 91%, Fan Face Location, 2 o'clock Location; Configuration 31.

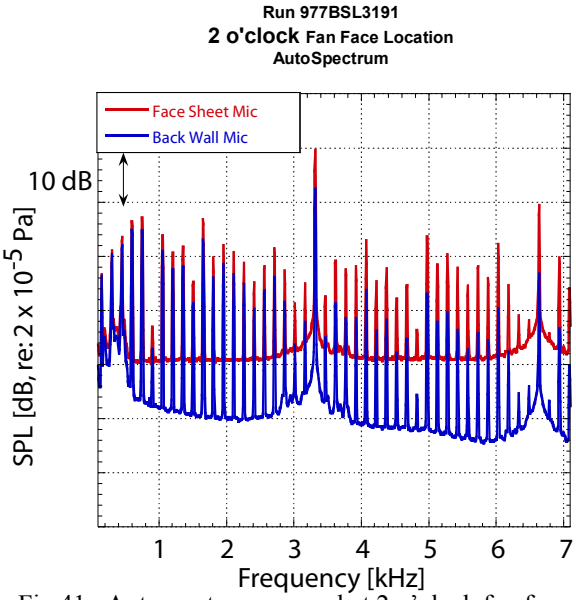

Fig 41. Autospectra measured at 2 o'clock fan face inlet location with face sheet and back wall mics shown at 91% engine power. Note that primary BPF is at 3320 Hz with many harmonics and rotor-stator interactions prominent.

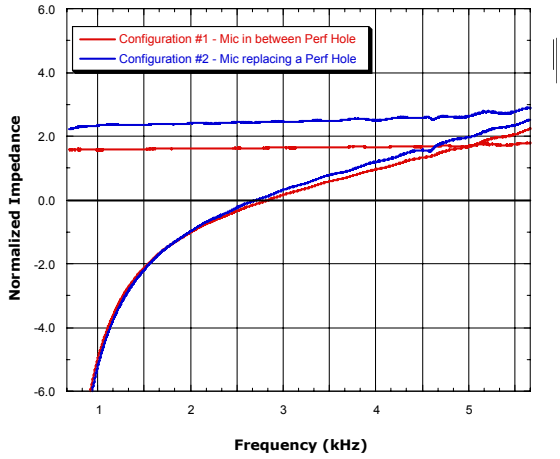

Fig 42. Effect of in-situ instrumentation: acoustic impedance with and without the face sheet mic in place of a perforate hole.

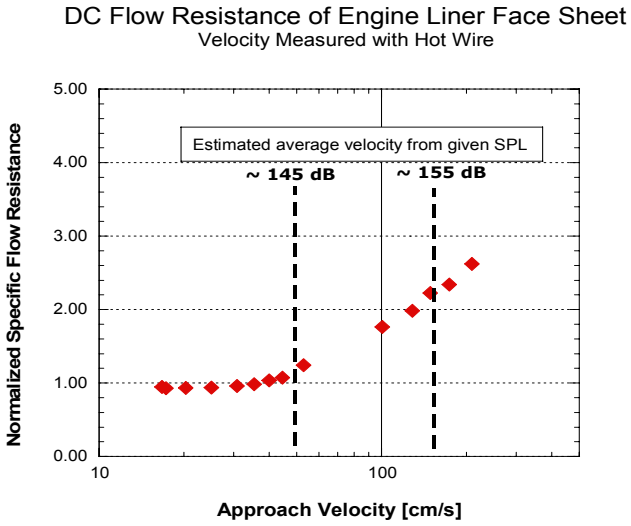

Fig 44. DC normalized flow resistance for liner face sheet.

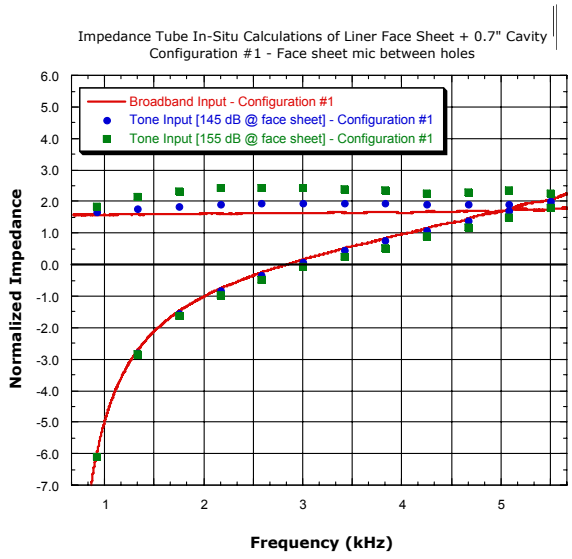

Fig 43. Effect of SPL on acoustic resistance.

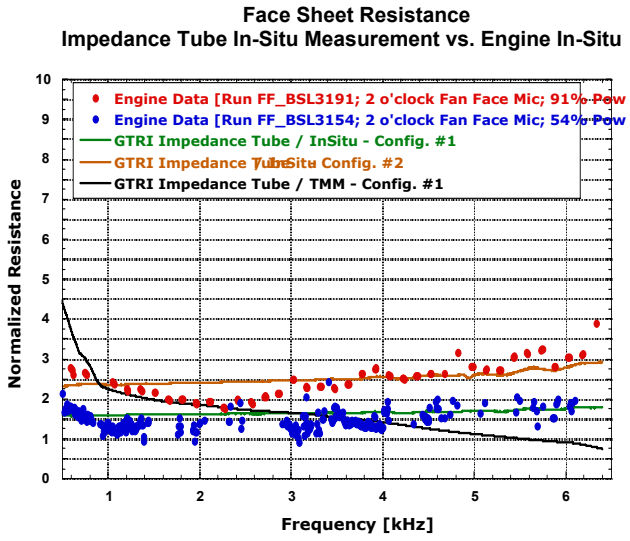

Fig 45. Comparison of face sheet resistance: Engine data vs. Impedance tube data.